Investigation of ETG Mode Micro Turbulence in FT-2 Tokamak

E.Z. Gusakov 1), A.D. Gurchenko 1), A.B. Altukhov 1), V.V. Bulanin 2), L.A. Esipov 1), M.Yu. Kantor 1), D.V. Kouprienko 1), S.I. Lashkul 1), A.V. Petrov 2), A.Yu. Stepanov 1)

1) Ioffe Physico-Technical Institute, 26 Polytekhnicheskaya, St.-Petersburg, Russia
2) SPbSPU, 29 Polytekhnicheskaya, St.-Petersburg, Russia

e-mail contact of main author: evgeniy.gusakov@mail.ioffe.ru

Abstract. The unique correlative upper hybrid resonance backscattering (UHR BS) technique is applied at the FT-2 tokamak for investigation of fine scale density fluctuations which are considered nowadays as a possible candidate for explanation of the anomalous ion and electron energy transport in magnetized fusion plasmas. The measurements are carried out in ohmic discharge at several values of plasma current and density and during current ramp up and lower hybrid heating experiments. The moveable focusing antennae set have been used in experiments allowing probing out off equatorial plane. The frequency and radial wave number spectra of small-scale component of tokamak turbulence are determined from the correlation data with high spatial resolution. Two small-scale modes possessing substantially different phase velocity are observed in plasma under conditions when the threshold for the ETG mode excitation is overcome. The possibility of plasma poloidal velocity profile determination using the UHR BS signal is demonstrated.

1. Introduction

Electrostatic fine scale electron temperature gradient (ETG) mode turbulence is discussed nowadays as a possible candidate for explanation of the anomalous electron energy transport in tokamak plasmas [1, 2]. In spite of the fact the theory predictions have not been checked yet experimentally, it is often used for description of anomalous electron transport and interpretation of experimental data. The lack of experimental data on the ETG turbulence is caused by its extremely small scale, complicating investigation with diagnostic tools (microwave reflectometry) presently used in tokamaks. Unlike the fluctuation reflectometry, the UHR BS technique is sensitive to the scales in the interval between ion and electron Larmor radii, where the excitation of the ETG mode is expected. In this paper the results of investigation of frequency and wave number spectra of small-scale component of tokamak plasma turbulence performed with the new experimental tool – correlative UHR BS diagnostics, are presented.

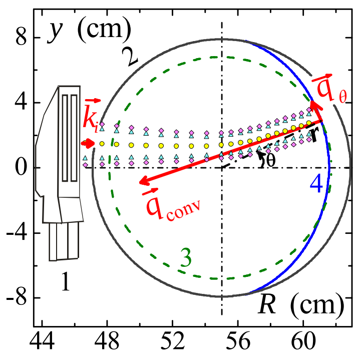

FIG. 1. FT-2 poloidal cross section: 1 – moveable antennae; 2 – limiter; 3 – magnetic surface; 4 – UHR; circles – central ray of the probing beam, triangles and rhombuses – probing beam at 1.5 dB and 3 dB power suppression levels.

2. The upper hybrid resonance backscattering technique

The upper hybrid resonance (UHR) backscattering (BS) technique or enhanced scattering [3] utilizes for local diagnostics of small-scale plasma fluctuations the effect of growth of wave vector and electric field of the probing extraordinary (*X*-mode) wave in the UHR, where condition $f_i^2 = f_{ce}^2(R) + f_{pe}^2(r)$ is fulfilled for the probing frequency f_i (R and r are tokamak major and minor radii, f_{ce} and f_{pe} are electron cyclotron and plasma frequencies, correspondingly). To provide the UHR accessibility in tokamak experiment the probing wave is launched from the high magnetic field side of the torus under conditions when the electron cyclotron resonance layer exists somewhere in a plasma. The UHR BS diagnostics benefits of the probing wave field and wave

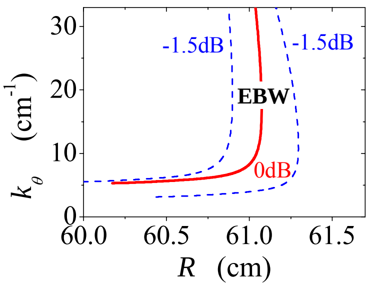

FIG. 2. Poloidal probing wave number growth near UHR along central ray (0 dB) and at -1.5 dB level.

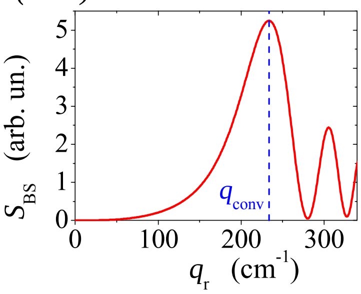

FIG. 3. UHR BS efficiency for central probing ray.

number growth leading to high localization, enhanced sensitivity to submillimetric scales and substantial frequency shift of the backscattered wave (Enhanced Doppler effect) [4-7]. According to [4, 5], in toroidal devices, where the UHR and magnetic surfaces do not coincide due to dependence of magnetic field on the major radius R (*FIG. 1*), the large probing wave vector component k_r, perpendicular to the UHR surface, has a finite projection onto the poloidal direction. In general case this projection is given by relation

$$k_\theta = k_{\theta 0} - k_r \left. \frac{\vec{e}_\theta \vec{e}_R f_{\rm ce}^2}{R\left|\vec{\nabla}(f_{\rm pe}^2 + f_{\rm ce}^2)\right|} \right|_{\rm UHR} , \qquad (1)$$

where $k_{\theta 0}$ gives the probing *X*-mode poloidal wave number out of the UHR zone, $\vec{e}_\theta$ and $\vec{e}_R$ are unit vectors in poloidal and major radius directions. This dependence was confirmed using beam tracing modelling in [6]. As it is shown in *FIG. 2* for the FT-2 tokamak experimental parameters, the poloidal wave number grows rapidly in the vicinity of the UHR surface. Its value there appears to be proportional to the vertical displacement of the ray trajectory. This dependence is justified in the outer discharge region close to the circular limiter, where we can transform expression (1) to the following simplified form [4, 5]

$$k_\theta \approx k_{\theta 0} + k_r \left. \frac{y}{r} \frac{f_{\rm ce}^2}{f_{\rm pe}^2} \frac{L_n}{R} \right|_{\rm UHR} , \qquad (2)$$

where y and r are a vertical displacement from the equatorial plane and minor radius of BS point at the UHR surface, correspondingly, and L_n is the density scale length. This projection, which can be much larger than the poloidal component of wave vector at the antenna, can lead to substantial enhancement of the Doppler frequency shift of the microwave BS by fluctuations moving with poloidal plasma flow. The corresponding frequency shift, according to (1), is given by

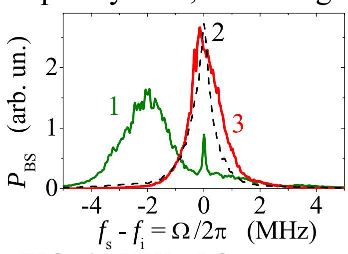

FIG. 4. UHR BS spectra (f_s – scattered frequency): 1 – y_a = 2 cm; 2 – 0 cm. Cutoff BS spectrum: 3 – y_a = 2 cm.

$$f_{\rm D} = 2\left[k_{\theta 0} + \frac{q_r}{2} \left. \frac{\vec{e}_\theta \vec{e}_R f_{\rm ce}^2}{R\left|\vec{\nabla}(f_{\rm pe}^2 + f_{\rm ce}^2)\right|} \right|_{\rm UHR} \right] V_\theta , \qquad (3)$$

where $V_\theta = V_{\rm ph} + V_{E\times B}$ is the fluctuation poloidal velocity in the laboratory reference system, $V_{E\times B}$ is the plasma drift velocity and $V_{\rm ph}$ is the fluctuation phase velocity in the reference system moving with plasma and $q_r = 2k_r$ is the fluctuation radial wave number.

According to [3], the UHR BS frequency spectrum is determined by the turbulence spectrum $|n|^2_{q_r,q_\theta,\Omega}$, UHR BS efficiency $S_{\rm BS}(q_r)$, as well as by the antenna beam power distribution on the UHR in the vertical direction $F^2 = \exp[-2(y - y_*)^2\rho^{-2}]$ and is given by an integral over poloidal and radial fluctuation wave number q_θ, q_r

$$P_{\rm BS}(\Omega) = \int I_{q_r,\Omega} dq_r = \int |n|^2_{q_r,q_\theta,\Omega} S_{\rm BS}(q_r) F^2(y) dq_\theta dq_r , \qquad (4)$$

Here we also assumed the following relation between poloidal wave number q_θ of fluctuations contributing to the backscattering and vertical displacement y of the point where it happens $q_\theta = (2k_{\theta*} + q_r \cos\psi_*)y/y_*$, which can be derived using equation (1) and the BS Bragg condition ($k_{\theta*}$ is poloidal wave number out of the UHR at the probing beam axis possessing vertical displacement y_*; ψ_* is the angle between UHR and magnetic surface there). The UHR BS technique is only sensitive to fluctuations possessing wavelength smaller than half probing wavelength. The UHR BS efficiency $S_{BS}(q_r)$ shown in *FIG. 3* for the FT-2 experiment parameters experiences a sharp maximum at the wave number $q_r \approx 2(2\pi f_{ce}/c)(c/V_{Te})^{1/2}$ which corresponds to BS in the linear conversion point [3].

3. Observation of the UHR BS signal at off equatorial plane probing

The experiment is performed at the FT-2 tokamak ($R_0 = 55$ cm, $a = 8$ cm, $B_t \approx 2.2$ T, $I_p \approx 23$ -35 kA, $T_e(0) \approx 500$ eV, $n_e(0) < 5\times10^{13}$ cm^{-3}), where a movable focusing double antennae set, shown in *FIG. 1*, allowing off equatorial plane plasma *X*-mode probing from high magnetic field side, was installed. The maximal vertical displacement of antennae is ±2 cm, whereas the diameter of the wave beam at the position of UHR, as measured in vacuum is 1.5 - 1.7 cm, depending on the probing frequency. The probing is performed in the frequency range 53 - 72 GHz at power level of 20 mW. The coupling of emitting and receiving antennae is less than 40 dB. The UHR position is scanned from $R = 59.5$ cm to 63 cm by the probing frequency variation.

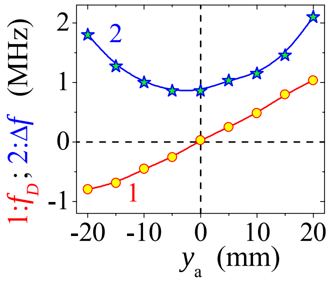

FIG. 5. Doppler frequency shift and spectral half-amplitude width versus antennae vertical displacement.

Just after the new antennae set installation a separate line less than 1.5 MHz wide and shifted by up to 2.5 MHz became routinely observable in the BS spectrum under condition of accessible UHR. The BS spectrum possessing 2 MHz shift, observed at 2 cm antenna vertical displacement, is shown in *FIG. 4* by curve 1. The amplitude of BS line there is higher than for the probing line because of enhancement of scattering cross section and small coupling of antennae horns. The ratio of the line frequency shift and broadening is larger than unity, which allows reliable determination of shift with high accuracy. The BS spectrum observed in equatorial plane and possessing no shift is shown in *FIG. 4* by curve 2. For comparison the BS spectra observed with the same antenna set, shifted by 2 cm from equatorial plane, under conditions when the UHR is not accessible is shown in *FIG. 4* by curve 3. This spectrum, which in fact corresponds to Doppler reflectometry with tilting angle of 15°, is only slightly shifted. The shift can be estimated only with poor accuracy at the level of 100 kHz. The line frequency shift proportionality to the vertical displacement of BS point predicted by equations (1) – (3) is confirmed in a special experiment in which the antennae shift from the equatorial plane was varied from discharge to discharge (*FIG. 5*). As it is seen the frequency shift (curve 1) of the BS satellite changes sign, when the antennae set crosses the equatorial plane. It appears also in *FIG. 5* that the BS line broadening (curve 2), which is approximately constant at small vertical displacement, grows approximately linearly with antenna vertical displacement. The observed BS spectra properties are consistent with the drift type spectrum of the turbulent fluctuations, which suffers from nonlinear broadening

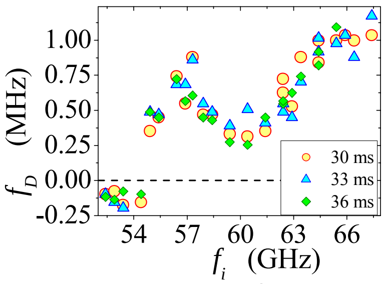

FIG. 6. Doppler frequency shift versus f_i.

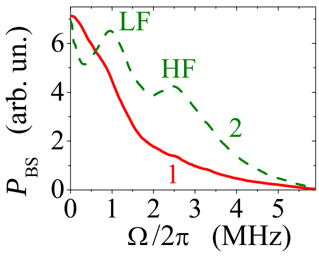

FIG. 7. UHR BS homodyne spectra: 1: 22 kA, 61.2 cm; 2: 32 kA, 60.6 cm.

$$|n|^2_{q_r,q_\theta,\Omega} = |n|^2_{q_r,q_\theta} \exp\left[-\frac{(q_\theta - \Omega/V_\theta)^2}{(\Delta q_\theta)^2}\right]\frac{\sqrt{\pi}}{\Delta q_\theta} \quad . \qquad (5)$$

The broadening parameter Δq_θ is supposed to be given by the relation: $\Delta q_\theta = (\delta_0 + \alpha q_\theta^2)^{1/2}$. The UHR BS satellite frequency shift dependence on the probing frequency and thus on the UHR position is non monotonic, as it is seen in *FIG. 6* for 32 kA discharge. It decreases with decreasing frequency, takes minimal value at $f_i = 60.5$ GHz, then maximal value at $f_i = 56.5$ GHz and finally change sign at $f_i = 54.5$ GHz. The last effect most likely indicates the change of rotation velocity direction, however to determine its exact value, according to (3) we need to calculate the position of BS point and measure the radial wavenumber, which will be done in section 5.

4. Observation of the ETG mode turbulence

Keeping in mind that the details of the correlation UHR BS technique developed at FT-2 tokamak were recently published in PPCF [8], we focus here on comparative analysis of results obtained in two FT-2 discharges.

In the first, 22 kA discharge, the He-puffing was performed for the spectroscopy diagnostic purposes, which resulted in a flat electron temperature profile at the edge. In this discharge the ETG mode threshold condition [2] $L_T < 1.25\, L_n$ (L_T, L_n are electron temperature and density scale length) was not overcome at minor radii $r > 6$ cm ($R > 61$ cm). The UHR BS homodyne spectrum obtained in this region (UHR position $R = 61.2$ cm, probing frequency 60.4 GHz) at $y_a = 1.5$ cm is shown in *FIG. 7* by curve 1. It consists of a single line with 1.2 MHz half-width at half-amplitude level. The wave number spectrum of turbulence in this point was investigated with the correlation technique [8]. Two BS signals at close probing frequencies f_i and $f_i + \Delta f_i$, measured simultaneously, were utilized for the cross-correlation function (CCF) computation. The normalized CCF dependence on Δf_i proportional to the UHR spatial separation ($\Delta R_{UH} = \Delta f_i\, \partial R_{UH}/\partial f_i$) was Fourier transformed. The obtained cross-correlation spectrum (CCS) was transformed into the UHR BS spectrum via multiplication by the frequency spectrum shown in *FIG. 7* by curve 1. The corresponding UHR BS spectrum $I_{q_r,\Omega}$ is shown in *FIG. 8(a)*.

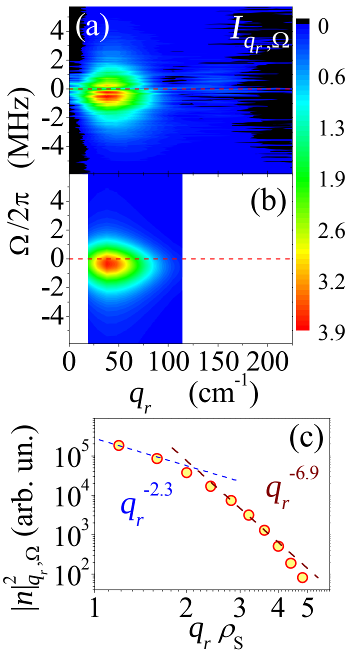

FIG. 8. (a) UHR BS spectrum obtained from CCS; (b) UHR BS spectral modelling result; (c) turbulence q_r spectrum reconstruction for I_p = 22 kA; R = 61.2 cm.

As a result of fitting procedure, based on equations (4) and (5), the following parameters were obtained in the case of figure 3(*b*): $V_\theta = 2.3 \pm 0.3$ km/s, $\Delta q_\theta = 37$ cm^{-1}. The wave numbers of fluctuations providing the maximal contribution to the BS signal are $q_r^{max} = 38$ cm^{-1}, $q_{\theta *} = q_\theta(y_*) = 12$ cm^{-1}. The UHR BS spectrum calculated for these parameters using expressions (4) and (5) is shown in *FIG. 8(b)*. As it is seen the modeling result nicely fits the experimental data. The turbulence q_r spectrum reconstructed in this case is demonstrated in *FIG. 8(c)* in double logarithmic scale ($\rho_S = \omega_{ci}^{-1}(T_e/m_i)^{1/2}$). It decays slowly as $q_r^{-2.3\pm0.7}$ for $1.1 < q_r\rho_S < 2.1$ and then steeply as $q_r^{-6.9\pm0.7}$ for $2.1 < q_r\rho_S < 5$. This

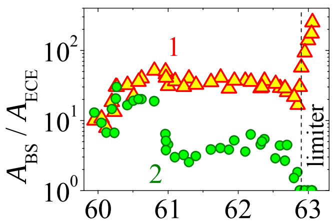

FIG. 9. 1 – LF and 2 – HF satellite's normalized spectral amplitudes profiles.

knee-like behavior is similar to that observed on Tore Supra tokamak for ITG mode turbulence [9].

In the second, 32 kA discharge, the necessary condition for the ETG mode excitation [2] ($L_T < 1.25\ L_n$) was fulfilled at $r > 4$ cm ($R > 59$ cm). The UHR BS homodyne spectrum obtained at $y_a = 1.5$ cm in this region for probing frequency 64.4 GHz (UHR position $R = 60.6$ cm) consists of two satellites, as it is shown by curve 2 in *FIG. 7* The amplitude of the low frequency (LF) satellite decreases when moving inward the plasma whereas the high frequency (HF) satellite's amplitude increases as it is shown in *FIG. 9*. The observation of a doublet in the UHR BS signal is most likely associated with simultaneous excitation of two different drift modes in the FT-2 plasma. To check this supposition and to identify modes correlation technique [8] was used. The UHR BS spectrum $I_{q_r,\Omega}$ obtained is shown in *FIG. 10(a)*. It consists of two components very different in frequency. The LF satellite at 1 MHz is larger there than the HF satellite at 2.4 MHz, which possesses higher q_r. Generally speaking, much higher wavenumber fluctuations contribute to this spectrum compared to that in *FIG. 8(a)*. To obtain the turbulence wave number spectrum $|n|^2_{q_r,q_\theta,\Omega}$ from this figure we supposed that it is a result of BS off two small-scale modes simultaneously excited in plasma and performed numerical modeling based on equations (4), (5). At first the fitting procedure was carried out for the LF spectral component and, as a result, its radial and poloidal wave numbers $q_r = 120$ cm^{-1}, $q_{\theta *} = q_\theta(y_*) = 23$ cm^{-1}, $\Delta q_\theta = 20$ cm^{-1} and phase velocity $V_\theta = 2.7 \pm 0.3$ km/s, were determined. After that the difference of the original spectrum and the outcome of the first fitting procedure was found, in which the second satellite dominates and a second fitting was performed. The determined radial and poloidal wave numbers and the broadening parameter are as follows: $q_r = 140$ cm^{-1}, $q_{\theta *} = q_\theta(y_*) = 27$ cm^{-1}, $\Delta q_\theta \approx 9$ cm^{-1} and phase velocity $V_\theta = 5.6 \pm 0.5$ km/s. The superposition of the two spectra reconstructed is shown in *FIG. 10(b)*. The radial wavenumber spectra obtained in the modeling for both satellites are shown in *FIG. 10(c)*. It is knee-like for the LF mode with the rupture point at $q_r\rho_S = 8$ and scales approximately as $q_r^{-2.5\pm0.8}$ for $2.8 < q_r\rho_S < 8$ and as $q_r^{-6.4\pm0.8}$ for $8 < q_r\rho_S < 15$. This mode may be probably identified with the small-scale ITG mode predicted in [10]. Unlike the LF spectrum, the HF component possesses a pronounced maximum at $q_r\rho_s = 9$ that corresponds to the radial wave length $\lambda_r = 27\rho_{ce}$. This spatial scale is close to the scale at which the ETG instability growth rate is maximal according to theory [11] ($\lambda_\theta = 20\rho_{ce}$). The dependence of the LF and HF satellite amplitudes on the fluctuation poloidal wave number appears to be quite different, as it is seen in *FIG. 11*. The LF satellite is maximal at $q_\theta = 0$ ($y_a = 0$ cm) whereas the HF satellite is suppressed at this position. Its amplitude increases with

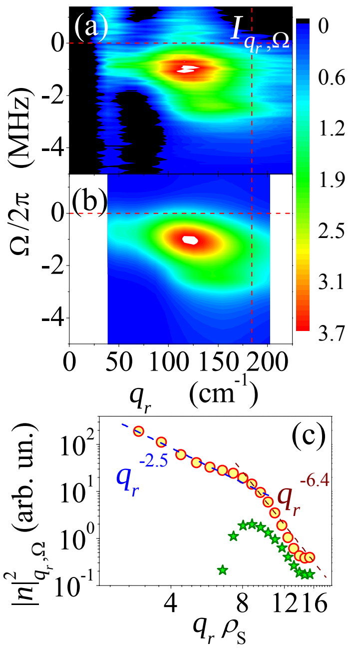

FIG. 10. (a) UHR BS spectrum obtained from CCS; (b) UHR BS spectral modelling result; (c) turbulence q_r spectrum reconstruction for $I_p = 32$ kA; $R = 60.6$ cm.

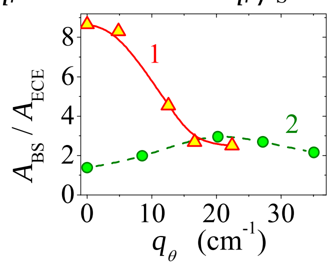

FIG. 11. Spectral amplitudes (1 – LF, 2 – HF) versus q_θ.

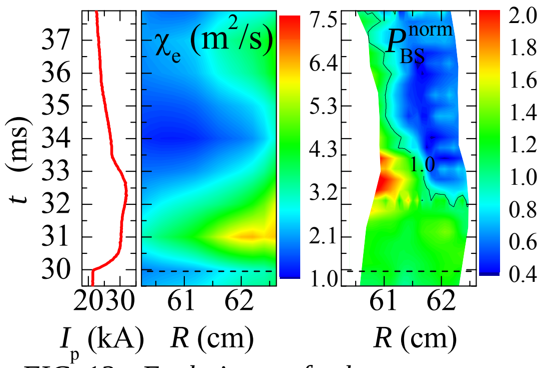

FIG. 12. Evolutions of plasma current, electron thermoconductivity profile and UHR BS signal profile (normalized to its value at 29 ms).

growing poloidal wave number.

According to results of wave number measurements, the UHR BS signal is produced by scattering off fine scale density fluctuations (millimetric and submillimetric scale), which are usually not supposed to dominate in the turbulence spectrum and determine the electron energy losses. Nevertheless, as the measurements performed in the FT-2 tokamak dynamical current ramp up experiment show, the evolution of the LF component of the UHR BS signal integrated in frequency range f_i – 1.6 MHz < < $f_s < f_i$ + 1.6 MHz is correlated to the behavior of electron thermal conductivity. The corresponding results are presented in *FIG. 12*. As it is seen there, at the 30th ms of the discharge the plasma current I_p was ramped from 22 kA up to 32 kA. This current increase was accompanied by the growth of electron thermal conductivity χ_e and the UHR BS signal P_{BS}, which lasted till the 32nd ms. After that a substantial suppression of both thermal conductivity and the UHR BS signal is observed till 37th ms. A similar correlation of the thermal conductivity and the UHR BS LF component behavior was observed at FT-2 in the lower hybrid heating experiment [12]. Unlike the LF component, the HF component behavior in these dynamical experiments was rather sensitive to the variation of density and temperature profiles than correlated to the electron anomalous transport coefficients. As it is seen in *FIG. 13a*, enhancement of the HF component of the UHR BS spectrum (integrated in the range $f_i - 6$ MHz $< f_s < f_i - 2$ MHz is only observed during the LHH experiment at 30 ms $<t<$34 ms for $r < 6.5$ cm when and where the ETG instability threshold condition [2] $L_T < 1.25\,L_n$ is satisfied (see *FIG. 13b and c*). After the RF pulse when the ETG instability condition is definitely violated, the HF component is suppressed all over the observation volume.

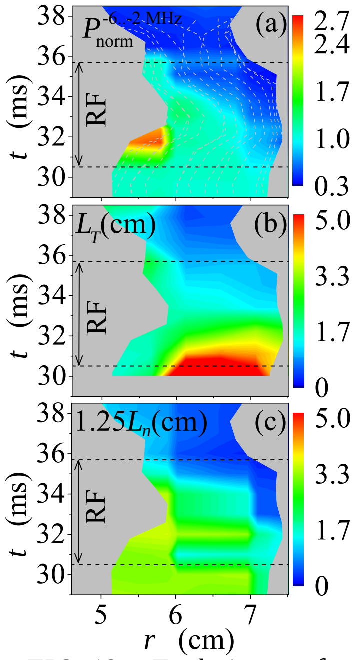

FIG. 13. Evolutions of (a) UHR BS normalized signal profile; (b) L_T ; (c) 1.25L_n

Based on these observations we may conclude that the small-scale fluctuations seen at high frequency are most likely directly excited due to the ETG instability. It is worth mentioning that the HF mode frequency and poloidal wave number spectral width, both absolute and relative are substantially smaller than that of the LF mode, which is probably explained by the HF mode being close to the excitation threshold. Based on the experimental results we are not able to confirm any role of the HF component in the electron transport so far. On contrary, the behavior of small scale LF mode also seen with the UHR BS diagnostics is correlated with the electron thermal conductivity.

5. Plasma rotation measurements by the UHR BS technique

According to theoretical expectations [13], the phase velocity of drift waves responsible for BS is given by the following expression

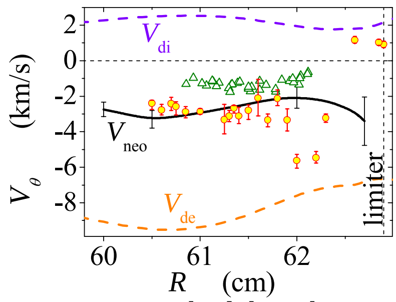

FIG. 14. Poloidal velocity profiles for 32 kA discharge: circles – UHR BS; triangles – Doppler reflectometry.

$$V_{ph} = V_{dr}\left[1+\left(q_\theta^2+q_r^2\right)\rho_s^2\right]^{-1} , \qquad (6)$$

where V_{dr} is the drift wave phase velocity at, $(q_\theta^2+q_r^2)\rho_s^2 << 1$ which is proportional to gradients of plasma parameters and depends on the drift mode type. According to (6) the phase velocity quickly decreases with growing wave number at $(q_\theta^2+q_r^2)\rho_s^2 >> 1$. Thus it can be beneficial for the plasma poloidal velocity diagnostics to use the UHR BS signal, which is produced by the small-scale turbulence component, possessing wavenumber in the range $(q_\theta^2+q_r^2)\rho_s^2 >> 1$. To determine the rotation velocity profile from the dependence of the Doppler frequency shift on the probing frequency, we need to know the electron density profile and, according to (3), to calculate the position of BS point and measure the radial wavenumber of fluctuations providing the largest contribution to the UHR BS signal with the correlation technique described above. In the case of frequency shift distribution shown for 32 kA discharge in *FIG. 6* the poloidal velocity profile takes the form shown in *FIG. 14* by circles. As it is seen, in the inner discharge zone plasma rotates in the electron diamagnetic drift direction at typical value 3 km/s, which is close to the value provided by the neoclassical theory [14] formula $V_{neo} \approx c\frac{T_i}{eB}\left[\frac{\partial(\ln n_e)}{\partial r}+(1-k)\frac{\partial(\ln T_i)}{\partial r}\right]$. At $R \approx 62$ cm the rotation velocity increases and than in the nearest vicinity of LCFS, at $R \approx 62.4$ cm the rotation velocity quickly decreases and changes sign in the edge region, where it is natural to expect positive plasma radial electric field, caused by fast electron losses along open magnetic field lines. The rotation velocity measured in the same discharge by Doppler reflectometry [15, 16] utilizing *O*-mode probing from low magnetic field side at frequencies in 28 GHz frequency band is shown in *FIG. 14* by triangles. The typical value given by this technique is 1.5 km/s which is substantially smaller than that provided by the UHR BS technique. The difference, according to expression (1), may be attributed to the contribution of the long-scale fluctuation phase velocity which is negative and close to the ion diamagnetic drift velocity V_{di} shown by the upper broken line in the *FIG. 14*.

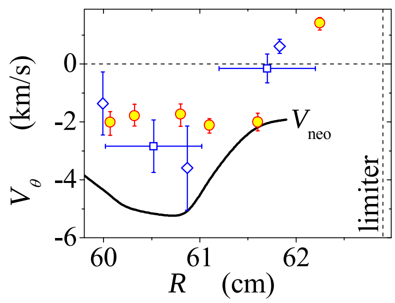

FIG. 15. Poloidal velocity profiles for I_p = 22 kA discharge with additional He-puffing: circles – UHR BS, squares – CIII-spectroscopy, rhombuses – HeII-spectroscopy.

The plasma rotation profile provided by the UHR BS technique was benchmarked as well against the visible light impurity spectroscopy [17] data. For this purpose the measurements were performed during the He-puffing into the optical diagnostic cross section, which resulted in the spectral lines emission growth. The comparison of rotation profiles obtained by the two techniques in the 22 kA discharge is shown in *FIG. 15*. As it is seen, within large error bars of spectroscopy point's profiles look similar. It should be stressed that both techniques indicate the change of rotation direction at the very edge of the tokamak discharge.

5. Conclusions

Summarizing results of the paper we would like to state that application of the correlation UHR BS diagnostics utilizing off equatorial plane probing to investigation of tokamak micro-turbulence is proved to be fruitful and opens numerous new possibilities. It is shown that small-scale turbulence possessing spatial scale much smaller than ion gyro-radius is excited at a measurable level in tokamak plasma. In the case the ETG mode instability condition is not fulfilled at the plasma edge a low frequency mode (most likely collisional drift wave) possessing a knee-like wave number spectrum is observed. In the opposite case, when the ETG mode instability condition $L_T < 1.25\, L_n$ is fulfilled, a doublet is observed in the UHR BS frequency spectrum. The low frequency satellite is similar to that observed at the edge. It is also characterized by a knee-like wave number spectrum, with a rupture point however shifted to smaller scales. The high frequency satellite possessing higher radial wave number and much higher phase velocity is identified as the ETG mode. It is shown that behavior of the low frequency component of the UHR BS signal in the current ramp up and LHH experiments at the FT-2 tokamak is correlated to the evolution of electron thermal conductivity. A possibility to apply the UHR BS to localized study of poloidal plasma rotation is demonstrated. The systematic excess of the rotation velocity over that provided by the Doppler reflectometry is explained by the contribution of the fluctuation phase velocity in the later case.

Acknowledgments

Financial support of RFBR grants 04-02-16534, 05-02-16569, 05-02-17761, 06-02-16785, NWO-RFBR grant 047.016.015 and INTAS grant 05-1000008-8046 is acknowledged.

References

[1] Jenko, F., et al., Phys. Plasmas **7** (2000) 1904.
[2] Jenko, F., Dorland, W., Hammett, G.W., Phys. Plasmas **8** (2001) 4096.
[3] Novik, K.M., Piliya, A.D., Plasma Phys. Control. Fusion **35** (1994) 357.
[4] Gurchenko, A.D., et al., Proc. 26 EPS Conf. on Control. Fusion and Plasma Phys., Maastricht (1999), ECA 23J, p.37.
[5] Bulyiginskiy D.G., et al., Phys. Plasmas **8** (2001) 2224.
[6] Altukhov, A.B., et al., Proc. 31 EPS Conf. on Control. Fusion and Plasma Phys., London (2004), ECA 28B, P-1.173.
[7] Altukhov, A.B., et al., Proc. 30 EPS Conf. on Control. Fusion and Plasma Phys., St.-Petersburg (2003), ECA 27A, P-4.170pd.
[8] Gusakov, E.Z., et al., Plasma Phys. Control. Fusion **48** (2006) A371.
[9] Hennequin, P., et al., Plasma Phys. Control. Fusion **46** (2004) B121.
[10] Smolyakov, A.I., Yagi, M., Kishimoto, Y., Phys. Rev. Lett. **89** (2002) 125005.
[11] Lin, Z., et al., Proc. 20 IAEA Conf. on Fusion Energy, Vienna (2004), IAEA-CN/TH/8-4.
[12] Lashkul, S.I., et al., This conference, EX/P6-18.
[13] Horton, W., Rev. Mod. Phys. **71** (1999) 735.
[14] Hirshman, S.P., Sigmar, D.J., Nucl. Fusion **21** (1981) 1079.
[15] Altukhov, A.B., et al., Proc. 30 EPS Conf. on Control. Fusion and Plasma Phys., St.-Petersburg (2003), ECA 27A, P-2.57.
[16] Bulanin, V.V., et al., Plasma Phys. Rep. **26** (2000) 813.
[17] Lashkul, S.I., et al., Plasma Phys. Control. Fusion **44** (2002) 653.